Journal of Computational Mathematics, Vol.18, No.5, 2000, 521–540.

NUMERICAL SOLUTION OF THE UNSTEADY INCOMPRESSIBLE NAVIER–STOKES EQUATIONS ON THE CURVILINEAR HALF–STAGGERED MESH*[1)]

Lan-chieh Huang
(*Institute of Computational Mathematics and Scientific/Engineering Computing, Chinese Academy of Sciences, Beijing 100080, China*)

Abstract

In this paper, the Crank–Nicholson + component–consistent pressure correction method for the numerical solution of the unsteady incompressible Navier–Stokes equation of [1] on the rectangular half–staggered mesh has been extended to the curvilinear half–staggered mesh. The discrete projection, both for the projection step in the solution procedure and for the related differential–algebraic equations, has been carefully studied and verified. It is proved that the proposed method is also unconditionally (in Δt) nonlinearly stable on the curvilinear mesh, provided the mesh is not too skewed. It is seen that for problems with an outflow boundary, the half–staggered mesh is especially advantageous. Results of preliminary numerical experiments support these claims.

Key words: Unsteady incompressible Navier-Stokes equations, Curvilinear half–staggered mesh, Discrete projection.

1. Introduction

Let us consider the unsteady incompressible Navier–Stokes equations (INSE)

$$\frac{\partial \mathbf{w}}{\partial t} + (\mathbf{w} \cdot grad)\mathbf{w} + grad\ p = \frac{1}{Re} div\ grad\ \mathbf{w} \tag{1.1}$$

$$div\ \mathbf{w} = 0 \tag{1.2}$$

on a two–dimensional region Ω with boundary $\partial\Omega$. Here $\mathbf{w}$ is the velocity vector; in terms of its Cartesian components $\mathbf{w} = (u, v)^T$; p is the pressure. The initial condition is given as

$$\mathbf{w}|_{t=0} = \mathbf{w}^0 \quad \text{on } \Omega \tag{1.3}$$

satisfying (1.2). We are concerned mainly with the solid wall boundary condition

$$\mathbf{w} = \mathbf{w}_B \quad \text{on } \partial\Omega \quad \text{satisfying } \oint_{\partial\Omega} w_n ds = 0 \tag{1.4}$$

* Received November 19, 1997.
[1)]Supported by Projects 19472068 and 19772056 of the National Natural Science Foundation of China and the Laboratory of Scientific and Engineering Computing of the Institute of Computational Mathematics, the Chinese Academy of Sciences.

but we will also briefly discuss the outflow boundary condition. Note the convection term can also be written in conservative form $(\mathbf{w} \cdot grad)\mathbf{w} = div(\mathbf{ww})$, using (1.2).

The difficulty in the numerical solution of the above problem lies in that (1.1) and (1.2) are partial differential equations with constraint; i.e. the system of equations is not entirely evolutionary. The projection methods of [2], [3], and [4] have been widely used and have proven to be most efficient for this type of problems. However, it is not always very well understood and has caused a great deal of confusion, e.g. see [5], [6], and [7] for discussions of the numerical boundary layers in pressure. For spatial discretization, there are many finite element methods – the so–called mixed methods. But for high Re unsteady complex flow simulation, the finite difference methods are usually used. It may be surprising to those not in the immediate field that the finite difference discretization is almost exclusively done on the staggered mesh of [8] for practical computation. The reason is that on the half–staggered mesh or the general mesh, the centered difference scheme (for $grad\ p$ and $div\ \mathbf{w}$) is not "regular" and the numerical solution is not "smooth", see [9] and [10], mostly the pressure solution can be intractable.

Because many of the advantages of the staggered mesh are lost on its curvilinear counterpart, see [11], we have directed our efforts toward the half–staggered mesh of [12], see Fig. 1. This mesh retains some of the advantages of the staggered mesh and does not need half–interval differencing on points adjacent to the boundary. Its main advantage lies in that with both components of the velocity at the same point, their coordinate transformation, the discretization of (1.2), and the formation of boundary conditions become more intelligible. But the solution of the discrete Poisson equation for pressure (or pressure correction) in the projection step becomes troublesome, in that there is an added constraint for solution and in that the solution can have oscillations, see [13] and [14]. We have shown in [15] that the added constraint is of no serious consequences for many problems, and that the oscillations do not affect the discrete gradient of p, which is of our only concern. Furthermore, for simulation of high Re unsteady complex flow in rectangular regions, a fast solver for the discrete Poisson equation with the most straightforward finite difference approximation of $grad$ and div on the half–staggered mesh has been developed in [16]. It has proven to be very efficient in the numerical tests of [17] and [1]. We point out here that the half–staggered mesh has been used quite successfully in [18], but with a different procedure for projection, in which the divergence–free velocity is computed directly with a Galerkin approach.

We have chosen the pressure correction (PC) projection method of [4] because its equation for the auxiliary velocity is consisitent with (1.1), and hence the boundary condition (1.4) can be used. Also it retains the second order time accuracy of the underlying difference scheme, say the Crank–Nicolson (CN) scheme. However with the regular PC projection method, the "deviation" problem is sometimes encountered in practical computation. In [1], it is explained that with spatial discretization on a *fixed* mesh, the INSE becomes a system of differential–algebraic equations (DAE). For its solution to evolve along the correct branch, a consistency condition between the components (here $\mathbf{w}$ and p) of the solution must be satisfied. The PC projection method does not preserve this consisitency condition, and hence may lead to "deviation"

and produce erroneous results. An additional pressure solution from the consistency condition itself per time step will produce the correct numerical results. However, in [1] the component–consistent pressure correction (CCPC) projection method is proposed, which preserves a discrete form of the consistency condition involving pressure at one time level, and which requires just one solution of the discrete Poisson equation per time step. Numerical experiments show that for both the CN and the Runge–Kutta time stepping, the CCPC projection method leads to the correct numerical solution. It is also shown in [1] that for both the CN and the Runge–Kutta time stepping, the CCPC projection method is of second order time accuracy for $\mathbf{w}$ and of first order time accuracy for p, with the correct interpretation of the assumption that the right hand side functions of the DAE have bounded derivatives in some closed region of our interest.

In this paper, the CNMT2 + CCPC method (MT for the Temam scheme modified to the staggered or the half–staggered mesh, which uses an average of the non–conservative and the conservative forms of the convection term for stability), or simply the CN + CCPC method, of [1] is extended to the curvilinear half–staggered mesh. Our purpose is numerical simulation of high Re unsteady complex flow using sufficiently fine mesh and sufficiently small Δt. For such problems, the efficiency of the solution of the discrete Poisson equation is of utmost importance. With careful derivation, the matrix of the system of linear algebraic equations corresponding to the discrete Poisson equation is symmetric, and hence facilitates the development of fast solvers. Also in this paper, the discrete projection is clearly stated, with the boundary condition left open, and the discrete gradient of "pressure" defined only on the interior points as for computation. The validity of the projection is proved with its uniqueness depending only on the uniqueness of the discrete gradient of "pressure" from the discrete Poisson equation, which is also a part of computation. The particular case of the curvilinear half–staggered mesh is verified as [14] via transformation matrices. This paper also contains a brief discussion on the outflow boundary. It is seen that for problems with an outflow boundary, the half–staggered mesh is most advantageous, without any constraint or oscillation problems from the discrete Poisson equation.

In Section 2 we state the DAE and study the discrete projection. In Section 3 we describe the CN scheme in the ξ, η computational region and prove its unconditional (in Δt) stablity under certain mesh conditions. The CCPC projection method is stated and its validity indicated in Section 4. The treatment of outflow boundary conditions is included. Then in Section 5, preliminary numerical results are presented, which support the above claims. In Section 6, the concluding remarks are given.

2. DAE and Discrete Projection

Let the computational region be covered by a mesh with interior velocity points I, boundary points B, and interior pressure points I_0. Let the INSE with spatial discretization be denoted as

$$\frac{d\mathbf{w}}{dt} + \mathbf{f}(\mathbf{w}) + Gp = 0, \quad \text{on } I \tag{2.1}$$

$$\frac{d\mathbf{w}}{dt} - \mathbf{w}'_B = 0, \quad \text{on } B \tag{2.2}$$

$$D\mathbf{w} = 0, \quad \text{on } I_0 \tag{2.3}$$

where $\mathbf{f}$ is a nonlinear operator with $\mathbf{f}(\mathbf{w})$ approximating the convection and viscosity terms; G and D are linear operators corresponding respectively to *grad* and *div*. Let $\mathbf{W}$ be the vector with all the u and v on I and B as components, and P the vector with all the p on I_0 as components. Then (2.1)–(2.3) can be written as

$$\frac{d\mathbf{W}}{dt} + \mathbf{F}(\mathbf{W}, t) + \underline{G}P = 0 \tag{2.4}$$

$$\underline{D}\mathbf{W} = 0 \tag{2.5}$$

On a fixed mesh, $\mathbf{F}$ is just a nonlinear function, while $\underline{G}$ and $\underline{D}$ are linear functions. Note that the nonhomogeneous boundary condition is incorporated in $\mathbf{F}(\mathbf{W}, t)$ as a known function of t. Equations (2.4), (2.5) form a system of DAE of index 2. Taking the time derivative of the constraint condition (2.5) and substituting (2.4) gives

$$\underline{DG}P = -\underline{D}F \tag{2.6}$$

which is the consistency condition for components $\mathbf{W}$ and P of the solution of the DAE.

For example on the half–staggered mesh, see Fig. 1, $\mathbf{W}$ and $\mathbf{F}$ are $2(N + N_B)$ dimensional vectors, $\underline{G}$ is a $2(N+N_B) \times M$ matrix, and $\underline{D}$ is a $M \times 2(N+N_B)$ matrix. Now partition $\mathbf{W}$ as $(\mathbf{W}_I, \mathbf{W}_B)^T$; in Fig.1

$$\mathbf{W}_I = (u_{22}, u_{32}, u_{23}, u_{33}, v_{22}, v_{32}, v_{23}, v_{33})^T$$

For points of I_0 adjacent to the boundary $D\mathbf{w}$ involves $\mathbf{w}$ on I and on B, write

$$D\mathbf{w} = D_I\mathbf{w}_I + D_B\mathbf{w}_B$$

In particular, $D\mathbf{w} = D_I\mathbf{w}_I$ where $\mathbf{w}_B$ is not involved. From the above we form

$$\underline{D}\mathbf{W} = (\underline{D_I}, \underline{D_B}) \begin{pmatrix} \mathbf{W}_I \\ \mathbf{W}_B \end{pmatrix} = \underline{D_I}\mathbf{W}_I + \underline{D_B}\mathbf{W}_B$$

where $\underline{D_I}$ is a $M \times 2N$ matrix. We also form

$$\underline{G}P = \begin{pmatrix} \underline{G_I} \\ 0 \end{pmatrix} P = (\ldots, Gp, \ldots; \ldots, 0, \ldots)^T$$

where $\underline{G_I}$ is a $2N \times M$ matrix; the 0 entries are due to the fact that in (2.2) no explicit pressure term appears. This is the class of $\underline{G}P$ that is under consideration, thus Gp on the boundary is not explicitly involved in any way. Note that

$$\underline{DG} = \underline{D_I G_I}$$

Partition $\mathbf{F}$ as $\mathbf{W}$, from (2.2) we have $\mathbf{F} = (\mathbf{F}_I, -\mathbf{W}'_B)^T$ and $\underline{D}\mathbf{F} = \underline{D_I}\mathbf{F}_I - \underline{D_B}\mathbf{W}'_B$. Thus (2.6) can be written as

$$\underline{D_I G_I}P = -\underline{D_I}\mathbf{F}_I + \underline{D_B}\mathbf{W}'_B \tag{2.7}$$

It is the solution of this kind of systems of linear algebraic equations, or often called the discrete Poisson equations, which will define the discrete projection. (Note that neither

Gp nor p on the boundary is involved.) For the half–staggered mesh, the properties of the $M \times M$ matrix $\underline{L} = \underline{DG}$ and the existence and "uniqueness" of the solution of (2.7), or (2.6), are discussed in [10]. Here we assume its solution and give the discrete projection theorem, which is almost trivial. However, its corollary is of direct use for our problems.

Theorem 1. *Any vector* $\mathbf{V}$ *of a vector space* $\mathcal{V}$ *can be uniquely decomposed into*

$$\mathbf{V} = \mathbf{U} + \underline{G}\Phi \tag{2.8}$$

where $\underline{D}\mathbf{U} = 0$, *under the assumption that*

$$\underline{DG}\Phi = \underline{D}\mathbf{V} \tag{2.9}$$

has solution Φ *with* $\underline{G}\Phi$ *unique.*

Indeed, left multiplying (2.8) by $\underline{D}$ yields (2.9), which has solution Φ and thus $\underline{G}\Phi$. From (2.8), we obtain $\mathbf{U} = \mathbf{V} - \underline{G}\Phi$. Now suppose also $\mathbf{V} = \tilde{\mathbf{U}} + \underline{G}\tilde{\Phi}$ with $\underline{D}\tilde{\mathbf{U}} = 0$. Applying $\underline{D}$, we get $\underline{DG}\tilde{\Phi} = \underline{D}\mathbf{V}$, which is the same equation as (2.9). By the uniqueness of $\underline{G}\Phi$, we have the uniqueness of decomposition (2.8).

Now let $\mathcal{D}$ denote the subspace of $\mathcal{V}$ of $\mathbf{U}$ with $\underline{D}\mathbf{U} = 0$, and $\mathcal{G}$ the subspace of $\mathcal{V}$ of form $\underline{G}\Phi$. Thus, $\mathcal{V} = \mathcal{D} \oplus \mathcal{G}$. The above unique decomposition also defines a projection $\underline{\mathcal{P}} : \mathcal{V} \to \mathcal{V}$, $\underline{\mathcal{P}}$ is linear and $\underline{\mathcal{P}}^2 = \underline{\mathcal{P}}$, with

$$\mathcal{V} = \mathcal{R}(\underline{\mathcal{P}}) \oplus \mathcal{N}(\underline{\mathcal{P}})$$

where $\mathcal{R}(\underline{\mathcal{P}})$ denotes the range of $\underline{\mathcal{P}}$ and $\mathcal{N}(\underline{\mathcal{P}})$ the nullspace of $\underline{\mathcal{P}}$, (see for example [19] or [20]). We define $\underline{\mathcal{P}}$ by $\underline{\mathcal{P}}\mathbf{V} = \mathbf{U}$, then

$$\underline{\mathcal{P}}\mathbf{U} = \mathbf{U}, \quad \underline{\mathcal{P}}(\underline{G}P) = 0 \tag{2.10}$$

also for $\underline{\mathcal{Q}} = \underline{\mathcal{I}} - \underline{\mathcal{P}}$,

$$\underline{\mathcal{Q}}\mathbf{U} = 0, \quad \underline{\mathcal{Q}}(\underline{G}P) = \underline{G}P \tag{2.11}$$

$\underline{\mathcal{P}}$ is the projection of $\mathcal{V}$ on $\mathcal{D}$ along $\mathcal{G}$, and $\underline{\mathcal{Q}}$ is the projection of $\mathcal{V}$ on $\mathcal{G}$ along $\mathcal{D}$. When $\mathcal{D}$ is orthogonal to $\mathcal{G}$, i.e.

$$(\mathbf{U}, \Gamma) = 0 \quad \text{for all } \mathbf{U} \text{ in } \mathcal{D} \quad \text{and for all } \Gamma \text{ in } \mathcal{G} \tag{2.12}$$

then the projection is orthogonal and $\|\underline{\mathcal{P}}\| = 1$, see Fig. 2.

From the above discrete projection theorem we get the following:

Corollary 2. *Any vector field* $\mathbf{v}$ *on* $I + B$, *with (1)* $\mathbf{v}_B = \mathbf{u}_B$ *or (2)* $\mathbf{v}_B = \mathbf{u}_B + (G\phi)_B$, *can be uniquely decomposed into*

$$\mathbf{v} = \mathbf{u} + G\phi \quad \text{on } I \tag{2.13}$$

where $D\mathbf{u} = 0$, *under the assumption that*

$$DG\phi = D_I G_I \phi = D_I \mathbf{v}_I + D_B \mathbf{v}_B \tag{2.14}$$

has a solution ϕ *with* $G\phi$ *unique.*

Indeed, form V as $(\ldots, \mathbf{v}_I, \ldots; \ldots, \mathbf{a}_B, \ldots)^T$ where for (1) $\mathbf{a}_B = \mathbf{u}_B$, for (2) $\mathbf{a}_B = \mathbf{v}_B - (G\phi)_B$. Since (2.14) is just (2.9) in component form, we have unique decomposition

$$\begin{pmatrix} \mathbf{V}_I \\ \mathbf{A_B} \end{pmatrix} = \begin{pmatrix} \mathbf{U}_I \\ \mathbf{U}_B \end{pmatrix} + \begin{pmatrix} \underline{G_I}\Phi \\ 0 \end{pmatrix}$$

with $(\mathbf{U}_I, \mathbf{U}_B)^T$ in $\mathcal{D}$ and $(\underline{G_I}\Phi, 0)^T$ in $\mathcal{G}$.

Note that in the case of (1) $\mathbf{v}_B = \mathbf{u}_B$, the interior and the boundary expressions are not the same. This is the cause of the numerical boundary layers in pressure in the projection methods. For case (2) $\mathbf{v}_B = \mathbf{u}_B + (G\phi)_B$, the interior and the boundary expressions are the same and no numerical boundary layer results. Such is the situation for (2.1) and (2.2), the boundary equation (2.2) must be compatible with the interior equation (2.1), $\mathbf{v}_B - (G\phi)_B$ corresponds to $\mathbf{f}_B + (Gp)_B = -\mathbf{w}'_B$, and F is formed as $(\ldots, \mathbf{f}(\mathbf{w}), \ldots; \ldots, -\mathbf{w}'_B, \ldots)^T$.

We will indicate in Section 4 that for the half–staggered mesh, the solution of the discrete Poisson equation (2.14) with unique $G\phi$ will depend on certain conditions on $\mathbf{V}_B$ ($\mathbf{w}_B$ or $\mathbf{w}'_B$ of our problem). When these conditions are satisfied, the discrete projection is valid.

Then applying $\underline{\mathcal{Q}}$ and $\underline{\mathcal{P}}$ respectively to (2.4), we obtain

$$\underline{G}P = -\underline{\mathcal{Q}}F(\mathbf{W}, t) \tag{2.15}$$

and

$$\frac{d\mathbf{W}}{dt} + \underline{\mathcal{P}}\mathbf{F}(\mathbf{W}, t) = 0 \tag{2.16}$$

We remark that (2.15) can be used in place of (2.6) as the consistency condition for the components $\mathbf{W}$ and P of the solution. We note also that equation (2.16) involves only $\mathbf{W}$.

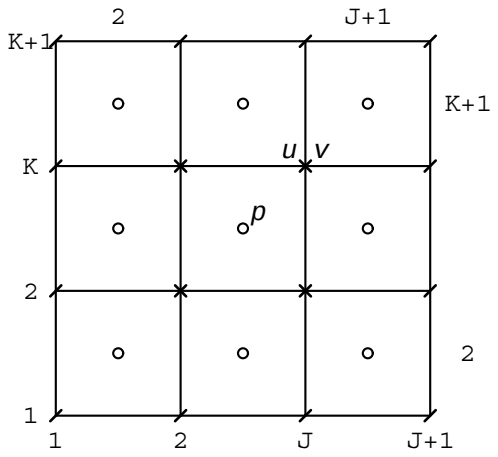

Figure 1. Half–Staggered Mesh
× I points (N)
/ B points (N_B)
∘ I_0 points (M)

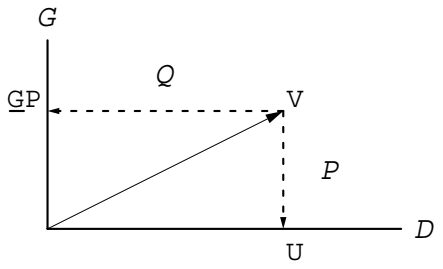

Figure 2. Orthogonal Projection

3. The Finite Difference Scheme on the Curvilinear Half–Staggered Mesh

The INSE in the Curvilinear Coordinate System

Let the curvilinear mesh on the physical region be generated by the smooth transformation functions

$$x = x(\xi, \eta) \quad y = y(\xi, \eta) \tag{3.1}$$

In the ξ, η plane the computational region is rectangular with uniform square mesh $\Delta\xi = \Delta\eta = 1$. The covariant base vectors of the curvilinear coordinate system are denoted as

$$\mathbf{g}_1 = \begin{pmatrix} x_\xi \\ y_\xi \end{pmatrix}, \quad \mathbf{g}_2 = \begin{pmatrix} x_\eta \\ y_\eta \end{pmatrix}$$

with

$$\sqrt{g} = x_\xi y_\eta - x_\eta y_\xi \tag{3.2}$$

the transformation Jacobian > 0. The contravariant vectors are denoted as

$$\mathbf{g}^1 = \begin{pmatrix} \xi_x \\ \xi_y \end{pmatrix} = \frac{1}{\sqrt{g}} \begin{pmatrix} y_\eta \\ -x_\eta \end{pmatrix}, \quad \mathbf{g}^2 = \begin{pmatrix} \eta_x \\ \eta_y \end{pmatrix} = \frac{1}{\sqrt{g}} \begin{pmatrix} -y_\xi \\ x_\xi \end{pmatrix} \tag{3.3}$$

Then the contravariant components of the velocity vector $\mathbf{w}$ are

$$w^1 = \mathbf{w} \cdot \mathbf{g}^1, \quad w^2 = \mathbf{w} \cdot \mathbf{g}^2 \tag{3.4}$$

and the continuity equation (1.2) becomes

$$\frac{1}{\sqrt{g}} \left[\frac{\partial}{\partial \xi} (\sqrt{g}\ w^1) + \frac{\partial}{\partial \eta} (\sqrt{g}\ w^2) \right] = 0 \tag{3.5}$$

with *div* in conservative form.

We write the momentum equation as

$$\frac{\partial \mathbf{w}}{\partial t} + \frac{1}{2} \left(w^1 \frac{\partial \mathbf{w}}{\partial \xi} + w^2 \frac{\partial \mathbf{w}}{\partial \eta} \right) + \frac{1}{2} \frac{1}{\sqrt{g}} \left[\frac{\partial}{\partial \xi} (\sqrt{g}\ w^1\ \mathbf{w}) + \frac{\partial}{\partial \eta} (\sqrt{g}\ w^2\ \mathbf{w}) \right] + \frac{\partial p}{\partial \xi}\ \mathbf{g}^1 + \frac{\partial p}{\partial \eta}\ \mathbf{g}^2$$

$$= \frac{1}{Re} \frac{1}{\sqrt{g}} \left[\frac{\partial}{\partial \xi} \left(\sqrt{g} g^{11} \frac{\partial \mathbf{w}}{\partial \xi} + \sqrt{g} g^{12} \frac{\partial \mathbf{w}}{\partial \eta} \right) + \frac{\partial}{\partial \eta} \left(\sqrt{g} g^{21} \frac{\partial \mathbf{w}}{\partial \xi} + \sqrt{g} g^{22} \frac{\partial \mathbf{w}}{\partial \eta} \right) \right] \tag{3.6}$$

Here convection is represented as an average of its non–conservative and its conservative forms, see [2] and [17]; this form with centered differencing leads to stability of the numerical scheme also on the curvilinear mesh, as we shall see shortly. The *grad p* is given in the non–conservative form for simplicity. With *div* in conservative form and *grad* in non–conservative form, the *div grad* has the standard simple form, see [21]. The momentum equation is a vector equation, there are many ways to decompose it into scalar equations, see [22]. Here we choose the most direct way, that is, to use just the Cartesian components of $\mathbf{w}$ and the base vectors.

Finite Difference Approximation of the INSE on the Half-Staggered Mesh

We consider first the geometric quantities. On each point of I and B, we approximate $x_\xi, y_\xi, x_\eta, y_\eta$ by centered finite differences over two intervals; they are respectively:

$$xc = \frac{\breve{\delta} x}{\Delta\xi} = \frac{x_{j+1k} - x_{j-1k}}{2\Delta\xi}, \quad yc = \frac{\breve{\delta} y}{\Delta\xi}, \quad xa = \frac{\breve{\delta} x}{\Delta\eta}, \quad ya = \frac{\breve{\delta} y}{\Delta\eta} \tag{3.7}$$

With these we compute

$$\begin{aligned} s &= xc\ ya - xa\ yc &&\simeq \sqrt{g} \\ A &= \frac{1}{s}((xa)^2 + (ya)^2) &&\simeq sg^{11} \\ B &= \frac{1}{s}(xc\ xa + yc\ ya) &&\simeq sg^{12} = sg^{21} \\ C &= \frac{1}{s}((xc)^2 + (yc)^2) &&\simeq sg^{22} \end{aligned} \tag{3.8}$$

We note that analogous to $g^{11}g^{22} - (g^{12})^2 > 0$ for $\sqrt{g} > 0$, we have

$$AC - B^2 > 0$$

for $s > 0$, which we assume to be true.

We come next to the continuity equation, it is approximated by

$$\bar{D}\mathbf{w} = \frac{1}{s}\bar{D}\mathbf{w} = \frac{1}{s}\left[\frac{\bar{\delta}}{\Delta\xi}(u\ ya - v\ xa) + \frac{\bar{\delta}}{\Delta\eta}(-u\ yc + v\ xc)\right] = 0 \quad \text{on } I_0 \tag{3.9}$$

in which δ itself denotes the centered differencing over one mesh interval, and $\bar{\delta}$ denotes the average in k for differencing in j, and the average in j for differencing in k. We can also write (3.9) as

$$\begin{aligned} &\bar{D}\mathbf{w} = \frac{\bar{\delta}V^1}{\Delta\xi} + \frac{\bar{\delta}V^2}{\Delta\eta} = 0 \quad \text{where} \\ &V^1 = u\ ya - v\ xa, \qquad V^2 = -u\ yc + v\ xc \end{aligned} \tag{3.10}$$

From (3.9), it is seen that the geometric quantities do not satisfy the "closed cell" condition (see [23]), i.e. for u = constant and v = constant, $\bar{D}\mathbf{w} \neq 0$. Using an η $(1, 2, 1)/4$ average for xc etc. will correct the situation; but this may not be necessary for fine curvilinear meshes generated by smooth transformation functions.

Now we give the CN finite difference approximation of the momentum equations in components u and v. To simplify the notation, we denote $u^{n+\frac{1}{2}} = \dfrac{u^n + u^{n+1}}{2}$ by u, etc.

$$\begin{aligned} &\frac{u^{n+1} - u^n}{\Delta t} + \frac{1}{2}\left(w^1\frac{\breve{\delta}u}{\Delta\xi} + w^2\frac{\breve{\delta}u}{\Delta\eta}\right) + \frac{1}{2}\frac{1}{s}\left[\frac{\breve{\delta}}{\Delta\xi}(s\ w^1\ u) + \frac{\breve{\delta}}{\Delta\eta}(s\ w^2\ u)\right] + \frac{1}{s}\left[\frac{\bar{\delta}p}{\Delta\xi}\ ya - \frac{\bar{\delta}p}{\Delta\eta}\ yc\right] \\ &\qquad = \frac{1}{Re}\frac{1}{s}\left[\frac{\delta}{\Delta\xi}\left(A\frac{\delta u}{\Delta\xi} + B\overline{\frac{\delta u}{\Delta\eta}}\right) + \frac{\delta}{\Delta\eta}\left(B\overline{\frac{\delta u}{\Delta\xi}} + C\frac{\delta u}{\Delta\eta}\right)\right] \quad \text{on } I \end{aligned} \tag{3.11a}$$

$$\begin{aligned} &\frac{v^{n+1} - v^n}{\Delta t} + \frac{1}{2}\left(w^1\frac{\breve{\delta}v}{\Delta\xi} + w^2\frac{\breve{\delta}v}{\Delta\eta}\right) + \frac{1}{2}\frac{1}{s}\left[\frac{\breve{\delta}}{\Delta\xi}(s\ w^1\ v) + \frac{\breve{\delta}}{\Delta\eta}(s\ w^2\ v)\right] + \frac{1}{s}\left[-\frac{\bar{\delta}p}{\Delta\xi}\ xa + \frac{\bar{\delta}p}{\Delta\eta}\ xc\right] \\ &\qquad = \frac{1}{Re}\frac{1}{s}\left[\frac{\delta}{\Delta\xi}\left(A\frac{\delta v}{\Delta\xi} + B\overline{\frac{\delta v}{\Delta\eta}}\right) + \frac{\delta}{\Delta\eta}\left(B\overline{\frac{\delta v}{\Delta\xi}} + C\frac{\delta v}{\Delta\eta}\right)\right] \quad \text{on } I \end{aligned} \tag{3.11b}$$

Here $\overline{\delta u}$ denotes the average in k for differencing over two intervals in j, and the average in j for differencing over two intervals in k; i.e.

$$\left[\overline{\frac{\delta u}{\Delta\xi}}\right]_{j,k+\frac{1}{2}} = \frac{1}{2}\left(\frac{u_{j+1,k+1} - u_{j-1,k+1}}{2\Delta\xi} + \frac{u_{j+1,k} - u_{j-1,k}}{2\Delta\xi}\right)$$

$$\left[\overline{\frac{\delta u}{\Delta\eta}}\right]_{j+\frac{1}{2},k} = \frac{1}{2}\left(\frac{u_{j+1,k+1}-u_{j+1,k-1}}{2\Delta\eta}+\frac{u_{j,k+1}-u_{j,k-1}}{2\Delta\eta}\right)$$

Stability of the CN Scheme

Now we show that the above CN scheme is unconditionally (in Δt) nonlinearly stable, i.e. for zero boundary conditions $\|\mathbf{w}^{n+1}\| \le \|\mathbf{w}^n\|$, if the curvilinear mesh is not too skewed. We state first the following partial sum relations: for $f_1 = f_{L+1} = 0$, see Fig. 3,

(1) $\sum_l f_l\ \breve{\delta} g_l = -\sum_l \breve{\delta} f_l\ g_l$

(2) $\sum_l f_l\ \delta p_l = -\sum_{l_0} \delta f_{l_0}\ p_{l_0}$

(3) $\sum_l f_l\ (p_{l_0+1}+p_{l_0}) = \sum_{l_0}(f_l + f_{l-1})\ p_{l_0}$

Multiply (3.11a) by $u^{n+1}+u^n = 2u$ and form $\sum_I s\ \Delta\xi\ \Delta\eta$; the first sum is just

$$\frac{1}{\Delta t}\sum_I [(u^{n+1})^2 - (u^n)^2]\ s\ \Delta\xi\ \Delta\eta$$

The convection and pressure sums mimic the respective integrals of the continuous equation which can be easily shown to be zero by transforming back to the x, y coordinate system. Here we proceed directly. From the ξ convection terms,

$$\sum_I \left(w^1 u\frac{\breve{\delta} u}{\Delta\xi}+\frac{1}{s}u\frac{\breve{\delta}}{\Delta\xi}(s\ w^1\ u)\right)\ s\,\Delta\xi\,\Delta\eta = \sum_I \left(s w^1 u\frac{\breve{\delta} u}{\Delta\xi}+u\frac{\breve{\delta}}{\Delta\xi}(s\ w^1\ u)\right)\Delta\xi\,\Delta\eta = 0$$

by relation (1). Similarly for the η convection terms.

From the $\dfrac{\delta p}{\Delta\xi}$ term,

$$\begin{aligned}
&\textstyle\sum_{jk} 2u_{j,k}\frac{1}{s_{j,k}}\frac{1}{2}\left[\frac{\delta p_{j,k_0+1}}{\Delta\xi}+\frac{\delta p_{j,k_0}}{\Delta\xi}\right](ya)_{j,k}\ s_{j,k}\ \Delta\xi\ \Delta\eta\\
= &-\textstyle\sum_k\sum_{j_0}\left(\frac{\delta\ u\ ya}{\Delta\xi}\right)_{j_0,k}(p_{j_0,k_0+1}+p_{j_0,k_0})\ \Delta\xi\ \Delta\eta\\
= &-\textstyle\sum_{j_0,k_0}\left[\left(\frac{\delta\ u\ ya}{\Delta\xi}\right)_{j_0,k}+\left(\frac{\delta\ u\ ya}{\Delta\xi}\right)_{j_0,k-1}\right]p_{j_0,k_0}\ \Delta\xi\ \Delta\eta\\
= &-2\textstyle\sum_{I_0}\left(\frac{\bar{\delta}\ u\ ya}{\Delta\xi}\right)_{j_0,k_0} p_{j_0,k_0}\ \Delta\xi\ \Delta\eta
\end{aligned}$$

in which we have used in turn relations (2) and (3). We obtain a similar expression for the $\dfrac{\delta p}{\Delta\eta}$ term; and adding we get

$$-2\sum_{I_0}\left[\frac{\bar{\delta}}{\Delta\xi}(u\ ya)+\frac{\bar{\delta}}{\Delta\eta}(-u\ yc)\right]p\ \Delta\xi\ \Delta\eta$$

Note the $\dfrac{\bar{\delta}}{\Delta\xi}$ and $\dfrac{\bar{\delta}}{\Delta\eta}$ terms in the bracket are exactly the first parts of the $\dfrac{\bar{\delta}}{\Delta\xi}$ and $\dfrac{\bar{\delta}}{\Delta\eta}$ terms of $\bar{D}\mathbf{w}$ of (3.9). From (3.11b) we get the corresponding second parts, and hence the two sums add up to zero.

Now we discuss the sum from the viscosity term; this needs more attention because of the cross differences. By relation (2) the first $\frac{\delta}{\Delta\xi}$ sum

$$\frac{2}{Re}\sum_I\left[u\frac{\delta}{\Delta\xi}\left(A\frac{\delta u}{\Delta\xi}+B\overline{\frac{\delta u}{\Delta\eta}}\right)\right]\Delta\xi\ \Delta\eta=-\frac{2}{Re}\sum_{j_0}\sum_k\frac{\delta u}{\Delta\xi}\left(A\frac{\delta u}{\Delta\xi}+B\overline{\frac{\delta u}{\Delta\eta}}\right)\Delta\xi\ \Delta\eta$$

Similarly the second $\frac{\delta}{\Delta\eta}$ sum. Altogether we have

$$-\frac{2}{Re}\left[\sum_{j_0,k}\frac{\delta u}{\Delta\xi}\left(A\frac{\delta u}{\Delta\xi}+B\overline{\frac{\delta u}{\Delta\eta}}\right)\Delta\xi\ \Delta\eta+\sum_{j,k_0}\frac{\delta u}{\Delta\eta}\left(B\overline{\frac{\delta u}{\Delta\xi}}+C\frac{\delta u}{\Delta\eta}\right)\Delta\xi\ \Delta\eta\right]$$

If the curvilinear mesh is such that B is sufficiently small, i.e. the ξ and the η lines are not too skewed, or if the above sum is sufficiently close to

$$-\frac{2}{Re}\sum_I\left[A\left(\frac{\delta' u}{\Delta\xi}\right)^2+2B\left(\frac{\delta' u}{\Delta\xi}\right)\left(\frac{\delta' u}{\Delta\eta}\right)+C\left(\frac{\delta' u}{\Delta\eta}\right)^2\right]\Delta\xi\ \Delta\eta$$

for some suitably defined δ', then from $AC-B^2>0$, the sum is ≥ 0 and $-\frac{2}{Re}$ times the sum is ≤ 0.

Similarly for (3.11b).

Summing up, we have shown that $\sum_I[(u^{n+1})^2-(u^n)^2]\ s\ \Delta\xi\ \Delta\eta+\sum_I[(v^{n+1})^2-(v^n)^2]\ s\ \Delta\xi\ \Delta\eta\leq 0$. That is,

$$\|\mathbf{w}^{n+1}\|\leq\|\mathbf{w}^n\|$$

under the condition that the curvilinear coordinate lines are not too skewed, (or that the mesh is sufficiently fine).

The Outflow Boundary Condition

In this section we also include a brief account of the outflow boundary condition, say at the right boundary. It is straightforward to work with the "frozen coefficient" equations of (1.1) and (1.2),

$$\frac{\partial\dot{\mathbf{w}}}{\partial t}+u\frac{\partial\dot{\mathbf{w}}}{\partial x}+v\frac{\partial\dot{\mathbf{w}}}{\partial y}+grad\ \dot{p}=\frac{1}{Re}div\ grad\ \dot{\mathbf{w}}\tag{3.12}$$

$$div\ \dot{\mathbf{w}}=0\tag{3.13}$$

where $\dot{\mathbf{w}}=(\dot{u},\dot{v})^T$ is the small perturbation of $\mathbf{w}$, and where u and v are frozen as constants. Using the energy method, see [24], (here taking the dot product of (3.12) with $\dot{\mathbf{w}}$, integrating over Ω, and using (3.13),) we get

$$\oint_{\partial\Omega}\left(-w_n\dot{\mathbf{w}}\cdot\dot{\mathbf{w}}-2\dot{w}_n\ \dot{p}+\frac{2}{Re}\dot{\mathbf{w}}\cdot\frac{\partial\dot{\mathbf{w}}}{\partial n}\right)ds\leq 0$$

as the sufficient condition for non–increasing $\|\dot{\mathbf{w}}(t)\|$. The pointwise outflow boundary condition at the right boundary is

$$-w_n\left(\dot{u}^2+\dot{v}^2\right)-2\left[(\dot{u}n_1+\dot{v}n_2)\,\dot{p}-\frac{1}{Re}\left(\dot{u}\frac{\partial\dot{u}}{\partial n}+\dot{v}\frac{\partial\dot{u}}{\partial n}\right)\right]\leq 0\tag{3.14}$$

Since $w_n > 0$, the first term on the left hand side is < 0. Taking

$$\dot{p}n_1 - \frac{1}{Re}\frac{\partial \dot{u}}{\partial n} = 0 \quad \text{and} \quad \dot{p}n_2 - \frac{1}{Re}\frac{\partial \dot{v}}{\partial n} = 0 \quad \text{or}$$
$$pn_1 - \frac{1}{Re}\frac{\partial u}{\partial n} \quad \text{and} \quad pn_2 - \frac{1}{Re}\frac{\partial v}{\partial n} \quad \text{specified, as 0 say}$$

(3.14) is satisfied.

In the curvilinear coordinate system, the unit normal vector to a line $\xi = const.$ is $\mathbf{n} = \mathbf{g}^1/\sqrt{g^{11}}$ and the normal derivative to a line $\xi = const.$ is $(g^{11}\frac{\partial}{\partial \xi} + g^{12}\frac{\partial}{\partial \eta})/\sqrt{g^{11}}$, thus the outflow boundary condition becomes

$$\begin{aligned} p\xi_x - \frac{1}{Re}\left(g^{11}\frac{\partial u}{\partial \xi} + g^{12}\frac{\partial u}{\partial \eta}\right) = 0 \\ p\xi_y - \frac{1}{Re}\left(g^{11}\frac{\partial v}{\partial \xi} + g^{12}\frac{\partial v}{\partial \eta}\right) = 0 \end{aligned} \tag{3.15}$$

cancelling $1/\sqrt{g^{11}}$. The same outflow boundary condition can be derived from the "frozen coefficient" equations of (3.6), with the geometric quantities also frozen as constants. The condition (3.15) will be applied by regarding the geometric quantities as constants and taking p and $g^{11}\frac{\partial \mathbf{w}}{\partial \xi} + g^{12}\frac{\partial \mathbf{w}}{\partial \eta}$ to be zero outside the right boundary in the ξ difference approximations of the $grad\, p$ term and the viscosity term of (3.6). The convection terms of (3.6) will be approximated with upwind differencing and the $\frac{\partial p}{\partial \eta}$ and $\frac{\partial}{\partial \eta}(\sqrt{g}g^{12}\frac{\partial \mathbf{w}}{\partial \xi})$ terms will be approximated by η differences at neighboring points $(j_0 = J + 1)$ inside the computational region.

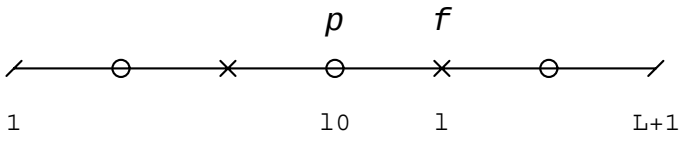

Figure 3. One–Dimensional Mesh

4. The Component-Consistent Presure Correction Projection Method

The Discrete Projection on the Curvilinear Half-Staggered Mesh

Let the time continuous version of (3.11) and (3.9) be written as DAE

$$\frac{d\mathbf{w}}{dt} + \tilde{\mathbf{f}}(\mathbf{w}) + \tilde{G}p = 0 \quad \text{on } I, \quad \mathbf{w} = \mathbf{w}_B \quad \text{on } B \tag{4.1}$$

$$\bar{D}\mathbf{w} = 0 \quad \text{on } I_0 \tag{4.2}$$

in which we have included the boundary conditon in the original form (1.4). All the results of Section 2 are valid with the understanding that all the G's and all the D's are changed to $\tilde{G}$'s and $\bar{D}$'s respectively. We keep the notation G and D for uniform mesh in the ξ, η computational region. Before stating the particular projection method, we recall from Corollary 2 that for the projection method to be valid, the discrete Poisson equation (2.14), here

$$\bar{D}\tilde{G}\phi = \bar{D}_I\tilde{G}_I\phi = \bar{D}\mathbf{v} \equiv \mathbf{rhs} \tag{4.3}$$

must have a solution ϕ with $\tilde{G}\phi$ unique. This problem is discussed thoroughly in [10]. It is shown there that

$$\underline{\bar{D}_I} = \underline{D_I R_I}, \quad \underline{\tilde{G}_I} = \underline{S_I^{-1} R_I^T G_I}$$

where the $2N \times 2N$ matrices $\underline{R_I}$ and $\underline{S_I}$ are

$$\underline{R_I} = \begin{pmatrix} diag(ya) & diag(-xa) \\ diag(-yc) & diag(xc) \end{pmatrix}, \quad \underline{S_I} = \begin{pmatrix} diag(s) & 0 \\ 0 & diag(s) \end{pmatrix},$$

and they are nonsingular because $s > 0$. It is also shown that the $M \times M$ matrix $\underline{\tilde{L}} = \underline{\bar{D}_I \tilde{G}_I}$ is symmetric and of rank $M-2$. Also the base vectors of $\mathcal{N}(\underline{\tilde{L}}) = \mathcal{N}(\underline{\tilde{L}}^T)$ can be represented as

$$\begin{aligned} \Psi_{01} &= (1,1,1\cdots;\cdots;\cdots;\ \cdots 1,1,1)^T \\ \Psi_{02} &= (1,-1,1\cdots;-1,1,-1\cdots;\cdots)^T \end{aligned}$$

The two constraints for (4.3) to have a solution are:

$$\Psi_{01}^T \mathbf{rhs} = 0, \quad \Psi_{02}^T \mathbf{rhs} = 0$$

Due to simple form of the **rhs**, see (3.10), the first constraint reduces to a relation involving the normal components of the velocity (**u** in Corollary 2) on the boundary, which approximates (1.4) satisfied by the boundary conditions of the INSE. The second constraint reduces to a relation involving the tangential components of the velocity on the boundary when the curvilinear mesh is orthogonal there. In general, it involves some component of the velocity on the boundary, see [10]. This constraint is entirely due to discretization, but for many problems (zero or constant boundary condition, symmetric region of solution, etc.) it does not present essential difficulties. The solution Φ of (4.3) has two degrees of freedom, i.e. $\Phi + c_1\Psi_{01} + c_2\Psi_{02}$ is also a solution. The Ψ_{01} term leads simply to uniqueness up to a constant and does not affect $\tilde{G}\phi$. The Ψ_{02} term leads to oscillations of equal amplitude in the solution, see [13] and [14]. Since $\underline{G}\Psi_{02} = 0$ ($\frac{\delta\psi}{\Delta\xi} = \frac{1}{2}(\psi_{j+1,k} - \psi_{j,k} + \psi_{j+1,k+1} - \psi_{j,k+1}) = \frac{1}{2}(1-(-1)+(-1)-1) = 0$, similarly $\frac{\delta\psi}{\Delta\eta} = 0$), $\underline{\tilde{G}}\Psi_{02} = 0$, and hence $\tilde{G}\phi$ is unique. Thus the discrete projection method, and similarly case (2) of Corollary 2, are valid.

We also note here the following skew–adjoint condition:

$$(\mathbf{v}, \tilde{G}\phi) = -(\bar{D}\mathbf{v}, \phi) \quad \text{for all } \phi \text{ and } \mathbf{v} \text{ with } \mathbf{v}_B = 0 \tag{4.4}$$

Indeed, the left hand side is

$$\sum_I \mathbf{v} \cdot \left(\frac{1}{s} R^T G\phi\right) s\Delta\xi\Delta\eta = \sum_I (R\mathbf{v}) \cdot G\phi \Delta\xi\Delta\eta = \sum_I V \cdot G\phi \ \Delta\xi\Delta\eta$$

where $R = \begin{pmatrix} ya & -xa \\ -yc & xc \end{pmatrix}$ and $V = (V^1, V^2)^T$ defined in (3.10). The right hand side is

$$-\sum_{I_0} \frac{1}{s} DR\mathbf{v} \ \phi \ s\Delta\xi\Delta\eta = -\sum_{I_0} DV \ \phi \ \Delta\xi\Delta\eta$$

Now it is easily seen that $\underline{G_I} = -\underline{D_I}^T$, thus

$$(\mathbf{V}_I, \underline{G_I}\Phi) = -(\underline{D_I}\mathbf{V}_I, \Phi)$$

Hence for $\mathbf{w}_B = 0$, which implies $V_B^1 = V_B^2 = 0$, we have

$$\sum_I V \cdot G\phi = -\sum_{I_0} DV\ \phi$$

and (4.4) is proved.

For $\tilde{D}\mathbf{u} = 0$, or $\bar{D}\mathbf{u} = 0$, we have the orthogonal relation $(\mathbf{u}, \tilde{G}\phi) = 0$. The space of $\mathbf{u}$ with $\bar{D}\mathbf{u} = 0$ and $\mathbf{u}_B = 0$ forms a subspace $\mathcal{D}_0$, projection $\underline{\mathcal{P}_0}$ on this space is orthogonal, see Fig. 2, and

$$\|\underline{\mathcal{P}_0}\| = 1 \tag{4.5}$$

Relation (4.4) and (4.5) are needed in the stability and convergence proofs for numerical schemes of our DAE, see [1].

The CCPC Projection Method

Now we consider the following CN time discretization of (4.1) and (4.2)

$$\frac{\mathbf{w}^{n+1} - \mathbf{w}^n}{\Delta t} + \tilde{\mathbf{f}}(\frac{\mathbf{w}^n + \mathbf{w}^{n+1}}{2}) + \tilde{G}p^{n+\frac{1}{2}} = 0 \quad \text{on } I, \quad \mathbf{w}^{n+1} = \mathbf{w}_B^{n+1} \quad \text{on } B \tag{4.6}$$

$$\bar{D}\mathbf{w}^{n+1} = 0 \quad \text{on } I_0 \tag{4.7}$$

The CCPC projection method proposed in [1] is

$$\frac{\tilde{\mathbf{w}}^{n+1} - \mathbf{w}^n}{\Delta t} + \tilde{\mathbf{f}}(\frac{\mathbf{w}^n + \tilde{\mathbf{w}}^{n+1}}{2}) + \tilde{G}p^{n-\frac{1}{2}} = 0, \quad \tilde{\mathbf{w}}^{n+1} = \mathbf{w}_B^{n+1} \quad \text{on } B \tag{4.8}$$

$$\frac{\mathbf{w}^{n+1} - \tilde{\mathbf{w}}^{n+1}}{\Delta t} + \tilde{G}\phi = 0, \quad \bar{D}\mathbf{w}^{n+1} = 0 \tag{4.9}$$

where $\tilde{\mathbf{w}}^{n+1}$ is the auxiliary velocity and $\phi = p^{n+\frac{1}{2}} - p^{n-\frac{1}{2}}$, the pressure correction. Equations (4.9) implies

$$\bar{D}\tilde{G}\phi = \frac{1}{\Delta t}(\bar{D}_I \tilde{\mathbf{w}}_I^{n+1} + \bar{D}_B \mathbf{w}_B^{n+1}) \tag{4.10}$$

The solution procedure is: (1) solve for $\tilde{\mathbf{w}}^{n+1}$ from (4.8) (at $n = 0$, $\tilde{G}p^0$ from the component–consistent condition is used), (2) solve for ϕ from (4.10), and (3) update $\mathbf{w}^{n+1}$ with the first equation of (4.9).

The validity of the projection step (4.9) is clear with the correlation of $\tilde{\mathbf{w}}^{n+1}$ with $\mathbf{v}$, $\mathbf{w}^{n+1}$ with $\mathbf{u}$, and $\Delta t\, \tilde{G}\phi$ with the $G\phi$ of Corollary 2. This projection method preserves the second order accuracy of the CN scheme; its intermediate step (4.8) is consistent with (4.1) and hence the original boundary condition can be used. It involves one Poisson solution per time step and does not lead to the "deviation" problem, see [1]. Here we just note that by adding (4.8) and (4.9) and applying $\underline{\mathcal{Q}}$ we get component–wise

$$\tilde{G}p^{n+\frac{1}{2}} = -\mathcal{Q}\tilde{\mathbf{f}}(\frac{\mathbf{w}^n + \tilde{\mathbf{w}}^{n+1}}{2})$$

which is an approximation involving p at one time level of (2.15), the consistency condition of $\mathbf{w}$ and p of DAE (4.1), (4.2).

In [1] it is shown that if the underlying evolutionary scheme is stable in the sense that $\|\mathbf{w}^{n+1}\| \leq \|\mathbf{w}^n\|$ with zero driving force, then the scheme with the CCPC projection method for INSE, with discrete *grad* and discrete *div* satisfying the skew–adjoint

condition (4.4), is stable with the norm $(\|\mathbf{w}\|^2 + \frac{\Delta t^2}{2}\|\tilde{G}p\|^2)^{\frac{1}{2}}$. From the discussion of stability of the CN scheme of Section 3, it is clear that our underlying scheme ((3.11) only as equation of $\mathbf{w}$, i.e. without the pressure terms) is stable under certain mesh conditions. Hence our CN scheme with the CCPC projection is stable under the same mesh conditions. It is also shown in [1] that the global time error (on fixed meshes as assumed) of our method is $O(\Delta t^2)$ for $\mathbf{w}$ and $O(\Delta t)$ for p.

What remains to be discussed is the solution for $\tilde{\mathbf{w}}^{n+1}$ from (4.8) by iteration, and for rectangular regions the iterative scheme is given in [17]. Here for the curvilinear mesh with cross differences in the viscosity term, the iterative scheme written for $\tilde{\mathbf{w}}^{n+\frac{1}{2}} = (\tilde{\mathbf{w}}^{n+1} + \mathbf{w}^n)/2$ is

$$\frac{\tilde{\mathbf{w}}^{(\nu+1)} - \mathbf{w}^n}{\Delta t/2} + C_\xi^{(\nu)}\tilde{\mathbf{w}}^{(\nu+1)} + C_\eta^{(\nu)}\tilde{\mathbf{w}}^{(\nu+1)} + E^{(\nu)} + Gp^{n-\frac{1}{2}} = 0 \tag{4.11}$$

in which $\tilde{\mathbf{w}}^{(\nu+1)}$ stands for the $(\nu+1)$st iterate of $\tilde{\mathbf{w}}^{n+\frac{1}{2}}$, $C_\xi^{(\nu)}$denotes the coefficient of $\tilde{\mathbf{w}}^{n+\frac{1}{2}}$ in the ξ convection term with w^1 at (ν) and in the ξ viscosity term; $C_\eta^{(\nu)}$ similarly. $E^{(\nu)}$ denotes the cross differences in the viscosity term. The delta form approximate factorization method is used for the solution of the iterative scheme (4.11) so that the boundary condition in (4.8) is still valid and so that upon convergence the local error is of $O(\Delta t^3)$. The resulting formulas are:

$$\begin{aligned}\left(I + \frac{\Delta t}{2}C_\xi^{(\nu)}\right)\Delta\tilde{\mathbf{w}}^{(\nu+\frac{1}{2})} &= -\frac{\Delta t}{2}(C_\xi^{(\nu)}\mathbf{w}^n + C_\eta^{(\nu)}\mathbf{w}^n + E^{(\nu)} + Gp^{n-\frac{1}{2}}) \\ \left(I + \frac{\Delta t}{2}C_\eta^{(\nu)}\right)\Delta\tilde{\mathbf{w}}^{(\nu+1)} &= \Delta\tilde{\mathbf{w}}^{(\nu+\frac{1}{2})}\end{aligned} \tag{4.12}$$

where $\Delta\tilde{\mathbf{w}} = \tilde{\mathbf{w}} - \mathbf{w}^n$. This iterative scheme is motivated by the fully implicit Temam scheme on the rectangular mesh (see [2] and [17]) and by the Beam–Warming delta form approximate factorization method with explicit cross differences terms (see [25]). Both of these schemes are stable in time n, corresponding here to the iterative solution being bounded in (ν). Preliminary numerical tests show the iterative scheme to be actually convergent.

Remark on Problems with an Outflow Boundary

Before presenting the results of numerical experiments on our method, we remark on the projection method for problems with an outflow boundary, see Fig. 4. Now u and v at the right boundary will be calculated from a difference approximation of equation (3.6) with outflow boundary condition (3.15). We state without proof that now $\tilde{L}$ is symmetric and of full rank. (Heuristically, the right outflow boundary condition includes almost the specification of p). Thus the discrete Poisson equation (2.9) has a unique solution and the discrete projection is valid. The CCPC solution procedure is as stated above, with I containing also the right boundary points. We note especially that for this type of problem, the advantages of the half–staggered mesh is fully realized without any constraint problems of the discrete Poisson equation.

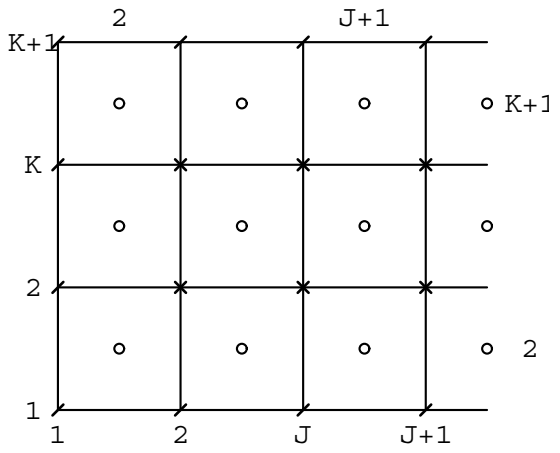

Figure 4. Mesh for Problems with Outflow Boundary

5. Preliminary Numerical Experiments

In this section we give the results of the preliminary numerical experiments on our CN + CCPC method on the curvilinear half–staggered mesh. The first example is the driven polar cavity flow from [26], which includes both experimental and numerical results. For this problem the polar coordinate system is obviously the most convenient physical coordinate system, but to test our method the Cartesian coordinates are chosen as the physical coordinates. The second example is the smooth expansion channel flow from [27], for which numerical results of an international workshop are available. This example is chosen to test our method with the non–orthogonal curvilinear mesh and with the outflow boundary condition.

Driven Polar Cavity Flow

Consider the polar cavity flow in a channel with inner radius 1 and outer radius 2, and $-0.5 \le \theta \le 0.5$, see Fig. 5. The left boundary conditions are $w_r = w_n = 0, w_\theta = w_\tau = -1$; as only orthogonal meshes are considered for this problem, $w_r = w^1/\sqrt{g^{11}}$ and $w_\theta = w^2/\sqrt{g^{22}}$; u and v are found from (3.3) and (3.4). The other boundary conditions and the initial condition are $u = v = 0$. Since $w_n = 0$ on the boundary, (1.4) or the first constraint condition for the solution of the discrete Poisson equation is obviously satisfied. If the non–uniform mesh is generated symmetric with respect to the x axis and with an odd K, then the second constraint condition is also satisfied.

With a 64×65 mesh ($\Delta r = 0.0078 - 0.0295, \Delta\theta = 0.0077 - 0.0290$), and $\Delta t = 0.1$, the steady–state solution for $Re = 350$ was obtained in 400 time steps ($|u^{n+1} - u^n| \simeq 0.7 \times 10^{-7}, |v^{n+1} - v^n| \simeq 0.9 \times 10^{-7}$). The streamlines are given in Fig. 6; the w_r and w_θ distributions on lines $\theta = -20^\circ, -10^\circ, 0^\circ, 10^\circ, 20^\circ$ are shown in Fig. 7. These results agree well with both the numerical and the experimental results shown in [26].

Smooth Expansion Channel Flow

Consider the flow in a planar channel with lower boundary

$$y_{low} = \frac{1}{2}\left[tanh\left(2 - \frac{30x}{Re}\right) - tanh(2)\right]$$

and with upper boundary $y_{up} = 1$, the plane of symmetry. For our purposes, we take $Re = 10$ because of its rather distorted geometry, see Fig. 8. At the lower wall boundary, the no–slip condition $u = v = 0$ is imposed; at the top boundary, the symmetry condition is used. At the left inlet boundary,

$$u = 3\left(z - \frac{z^2}{2}\right) \quad \text{where } z = \frac{y - y_{low}}{1 - y_{low}}, \quad v = 0$$

Here the fully developed Poiseuille flow condition has been adjusted to hold at $x = x_L$, much further left of the position $x = 0$ of the start of large expansion. At the right outlet boundary, the outflow boundary condition (3.15) is used as described in Section 3. Here $x_\xi = y_\eta = 0$, and the implementation is simplified.

The mesh is generated so that it is dense near the wall and near the starting point of large expansion of the channel. For $x_R = 6$ (and $x_L \simeq -1.4$), a 62×20 mesh ($\Delta x = 0.085 - 0.225, \Delta y = 0.033 - 0.085$ at $x = 0$) shown in Fig. 8 was used. With $\Delta t = 0.1$, the steady–state solution was obtained in 200 time steps ($|u^{n+1} - u^n| \simeq 0.6 \times 10^{-7}, |v^{n+1} - v^n| \simeq 0.1 \times 10^{-7}$). The pressure p adjacent to the wall is given in Fig. 9 (solid line); it is in accordance with the numerical result of [27] (dots, $x_R = Re/3$), – our concern being only with $\frac{\delta p}{\delta x}$. Note the obvious improvement near the start of expansion, due to the fully developed Poiseuille flow condition at inlet $x = x_L$, ($\frac{\partial y}{\partial x} = -0.247 \times 10^{-4}$). In [27], "the pressure has a singular point at the inlet" because this condition was "prescribed at the inlet, in spite of the non-zero slope of the wall at $x = 0$", ($\frac{\partial y}{\partial x} = -0.106$). The p distribution for $x_R = 4$ is also shown (dash line), its $\frac{\delta p}{\delta x}$ is also acceptable; however at the outlet $\frac{\delta p}{\delta x} = -0.363$ and -0.219 for $x_R = 6$ and 4 respectively, while $\frac{\partial p}{\partial x} = \frac{-3}{8\ Re} = -0.375$ for the fully developed Poiseuille flow. We also tried outflow boundary conditions: $p = 0$ and $\frac{\partial u}{\partial x} = \frac{\partial v}{\partial x} = 0$, the results were almost the same as those above. It is seen that our method also works well on skewed curvilinear half–staggered meshes and for problems with outflow boundaries.

We remark:

(1). Our preliminary numerical experiment is only to test the performance of our method with the curvilinear half–staggered mesh. We make no recommendation on the use of the CN scheme for steady–state problems. We propose our method for high Re unsteady complex flow simulation with sufficiently fine meshes and sufficiently small Δt.

(2). For the solution of the discrete Poisson equation on the curvilinear half–staggered mesh, just the Gauss–Seidel iteration method was used in our numerical experiment. For unsteady complex flow simulation, the multi–level one–way dissection method has been proposed and has proven to be most efficient for the flow around a circular cylinder with Re up to 9500 with rich vortex structures, see [28] and [10].

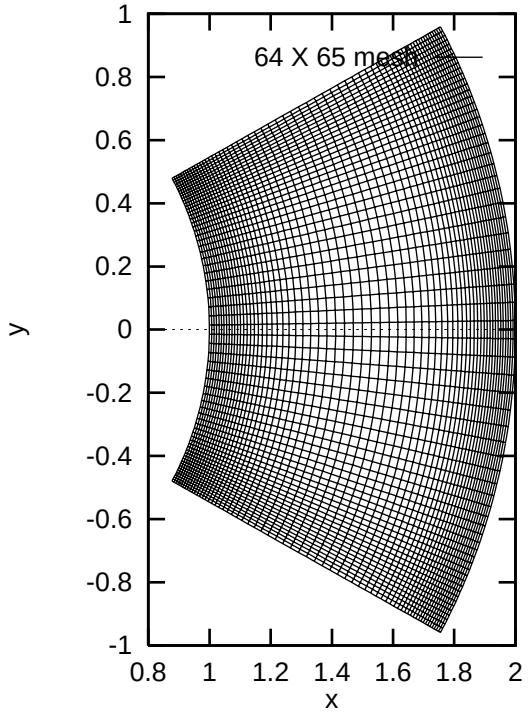

Figure 5. Driven Polar Cavity Flow–Mesh

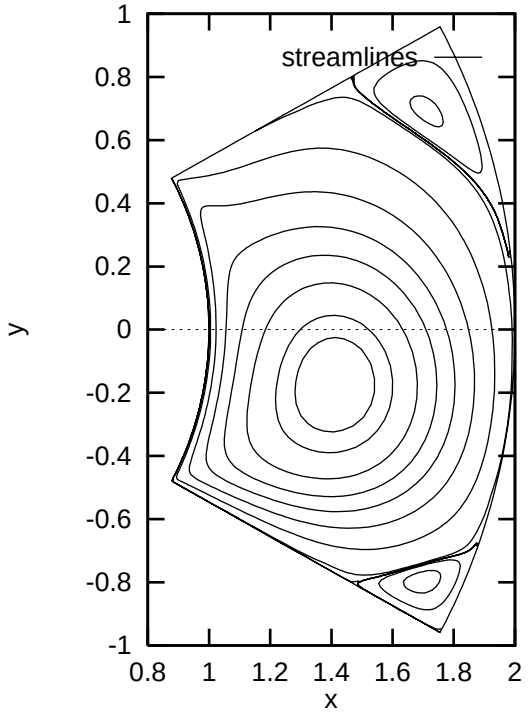

Figure 6. Driven Polar Cavity Flow–Streamlines

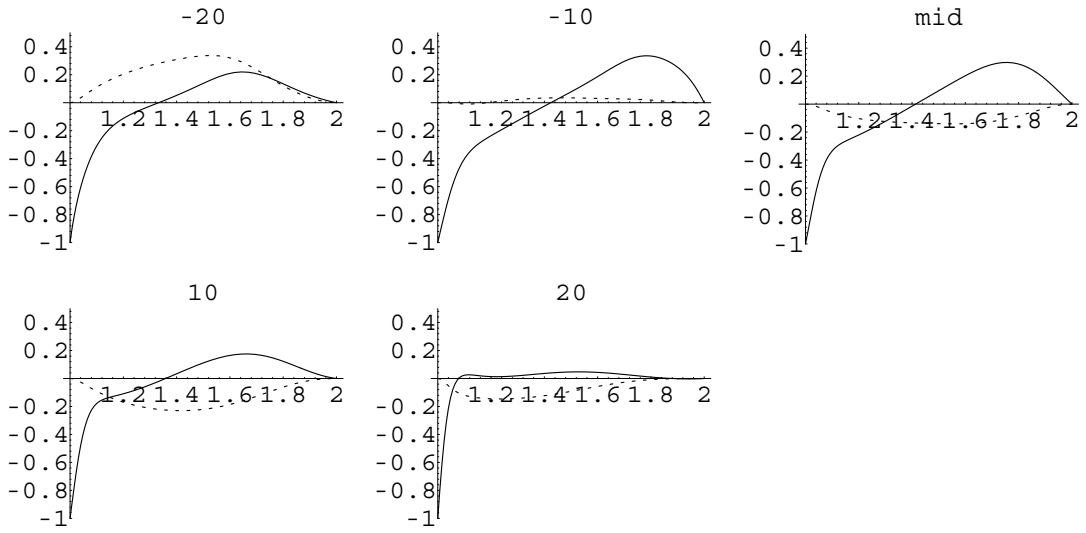

Figure 7. Driven Polar Cavity Flow – w_r, w_θ Distributions (solid line – w_θ, dash line – w_r)

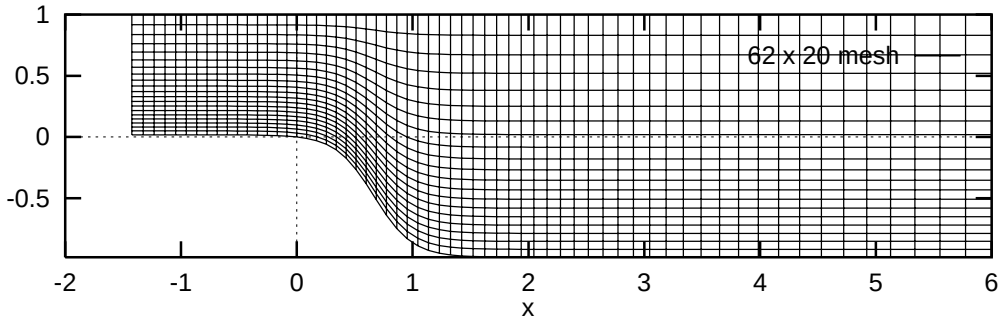

Figure 8. Smooth Expansion Channel Flow – Mesh

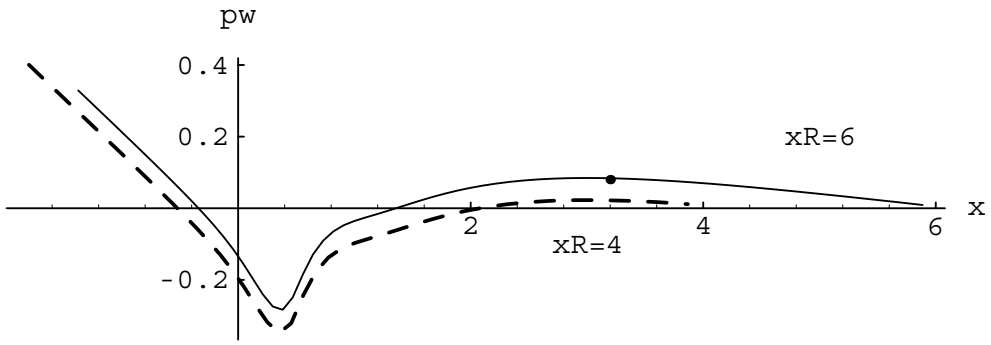

Figure 9. Smooth Expansion Channel Flow – pw Distributions

6. Conclusion

In this paper, the CN + CCPC method of [1] on the rectangular half–staggered mesh has been extended to the curvilinear half–staggered mesh. The discrete projection, both for the projection step in the solution procedure and for the related DAE, has been carefully studied and verified. It is proved that the method is also unconditionally (in Δt) nonlinearly stable on the curvilinear mesh, provided the mesh is not too skewed. It is also shown that for problems with an outflow boundary, the advantages of the half–staggered mesh are fully realized without any constraint problems or oscillation problems from the discrete Poisson equation. Results of preliminary numerical experiments support these claims.

A fast solver for the discrete Poisson equation on the curvilinear half–staggered mesh has been proposed in [28], and has proven to be most efficient in [10] for high Re unsteady complex flow simulation. Thus for the numerical solution of unsteady INSE in primitive variables, the half–staggered mesh is a viable alternative to the staggered mesh and is more advantageous than the latter in many instances.

Acknowledgement. The author would like to thank Prof. Zhang Guan Quan and Prof. Zhang Lin Bo for helpful discussions and valuable suggestions throughout our work.

References

[1] L.C. Huang, Y.D. Wu, The component–consistent pressure correction projection method for the incompressible Navier–Stokes equations, *Computer and Math. with Applic.,* **31** (1996), 1–21.

[2] R. Temam, Navier–Stokes Equations, Theory and Numerical Analysis, Elsevier Science Pub. B.V., New York, 1984.

[3] A.J. Chorin, Numerical solution of Navier–Stokes equations, *Math. Comput.,* **22** (1968), 745–762.

[4] J. van Kan, A second–order accurate pressure–correction scheme for viscous incompressible flow, *SIAM J. Sci. Stat. Comput.,* **7** (1986), 870–891.

[5] W.N. E, J.G. Liu, Projection method I: convergence and numerical boundary layers, *SIAM J. Num. Anal.,* **32** (1995), 1017–1057.

[6] R. Temam, Remark on the pressure boundary condition for the projection method, *Theoretical and Computational Fluid Dynamics,* **3** (1991), 181–184 .

[7] R. Rannacher, On Chorin's projection method for the incompressible Navier– Stokes equations, in Navier–Stokes Equations, Theory and Numerical Methods, J.G. Heywood et al. eds., Springer–Verlag, Berlin, 1992.

[8] F.H. Harlow, J.E. Welsh, Numerical calculation of time–dependent incompressible flow of fluid with free surface, *Phys. of Fluids,* **8** (1965), 2182-2189.

[9] J.C. Strikwerde, Finite difference methods for the Stokes and Navier–Stokes equations, *SIAM J. Sci. Stat. Comput.,* **5** (1984), 56–68.

[10] A. George, L.C. Huang, W.P. Tang, Y.D. Wu, Numerical simulation of high *Re* unsteady incompressible flow on the curvilinear half–staggered mesh, *SIAM J. Sci. Comput.,* to appear.

[11] W. Shyy, T.C. Vu, On the adoption of velocity variable and grid system for fluid flow computation in curvilinear coordinates, *J. Comput. Phys.,* **92** (1991), 82–105.

[12] M. Fortin, R. Peyret, R. Temam, Calcul des ecoulements d'un fluide visqueux incompressble, *J. Méc,* **10** (1971), 357–390.

[13] M. Fortin, An analysis of the convergence of mixed finite element methods, *Revue Française d'Automatique Informatique et Recherche Opérationelle,* **11** (1977), 341–354.

[14] A.B. Stephens et al., A finite difference Galerkin formulation for the incompressible Navier–Stokes equations, *J. Comput. Phys.,* **53** (1984), 152–172.

[15] L.C. Huang, Y.D. Wu, On the half-staggered mesh for the finite difference solution of the unsteady incompressible Navier–Stokes equations, *J. Comput. Math.,* **18** (1996), 24–37 (in Chinese).

[16] Golub G.H., Huang L.C., Simon H., Tang W.P., A fast Poisson solver for the finite difference solution of the incompressible Navier-Stokes equations, *SIAM J. Sci. Comput.,* **19** (1998), 1606–1624.

[17] L.C. Huang, Y.D. Wu, On efficient and robust finite difference schemes for the unsteady incompressible Navier-Stokes equations II, *Chinese J. Num. Math. & Applic.,* **19** (1997), 43–60.

[18] J.B. Bell, P.Colella, H.M. Glaz, A second-order projection method for the incompressible Navier–Stokes equations, *J. Comput. Phys.,* **85** (1989), 257–283.

[19] K. Hoffman, R. Kunze, Linear Algebra, Prentice–Hall, Inc., New Jersey, 1971.

[20] A.E. Taylor, D.E. Lay, Introduction to Functional Analysis, John Wiley & Sons, Inc., New York, 1980.

[21] A.I. Borisenko, I.E. Tarpov, Vector and Tensor Analysis, Dover Publications, Inc. New York, 1979.

[22] M. Vinokur, Conservation equations of gasdynamics in curvilinear coordinate systems, *J. Comput. Phys.,* **14** (1974), 105–125.

[23] M. Rosenfeld, D. Kwak, M. Vinokur, A fractional step solution for the unsteady incompressible Navier-Stokes equations in generalized coordinate systems, *J. Comput. Phys.,* **94** (1991), 102–137.

[24] J. Oliger, A. Sundström, Theoretical and practical aspects of some initial boundary value problems in fluid dynamics, *SIAM J. Appl. Math.,* **35** (1978), 419–446.

[25] R.M. Beam, R.F. Warming, Implicit Numerical Methods for the Compressible Navier Stokes and Euler Equations, Lecture Notes, CFD, von Karman Institute for Fluid Dynamics, 1982.

[26] L. Fuchs, N. Tillmark, Numerical and experimental study of driven flow in a polar cavity, *Int. J. Num. Meth. Fluids,* **5** (1985), 311–329.

[27] L. Davidson, P. Hedberg, Mathematical derivation of a finite volume formulation for laminar flow in complex geometries, *Int. J. Num. Meth. Fluids,* **9** (1989), 531–540.

[28] A. George, W.P. Tang, Y.D. Wu, Multilevel one–way dissection for unsteady incompressible Navier–Stokes flow, The 5th Ann. Conf. CFD Soc. of Canada, Victoria BC, Canada, 1997.